

Capability of the FoReRo2 instrument and the 2m RCC Telescope at the Bulgarian National Astronomical Observatory Rozhen for polarimetric observations of small solar system bodies



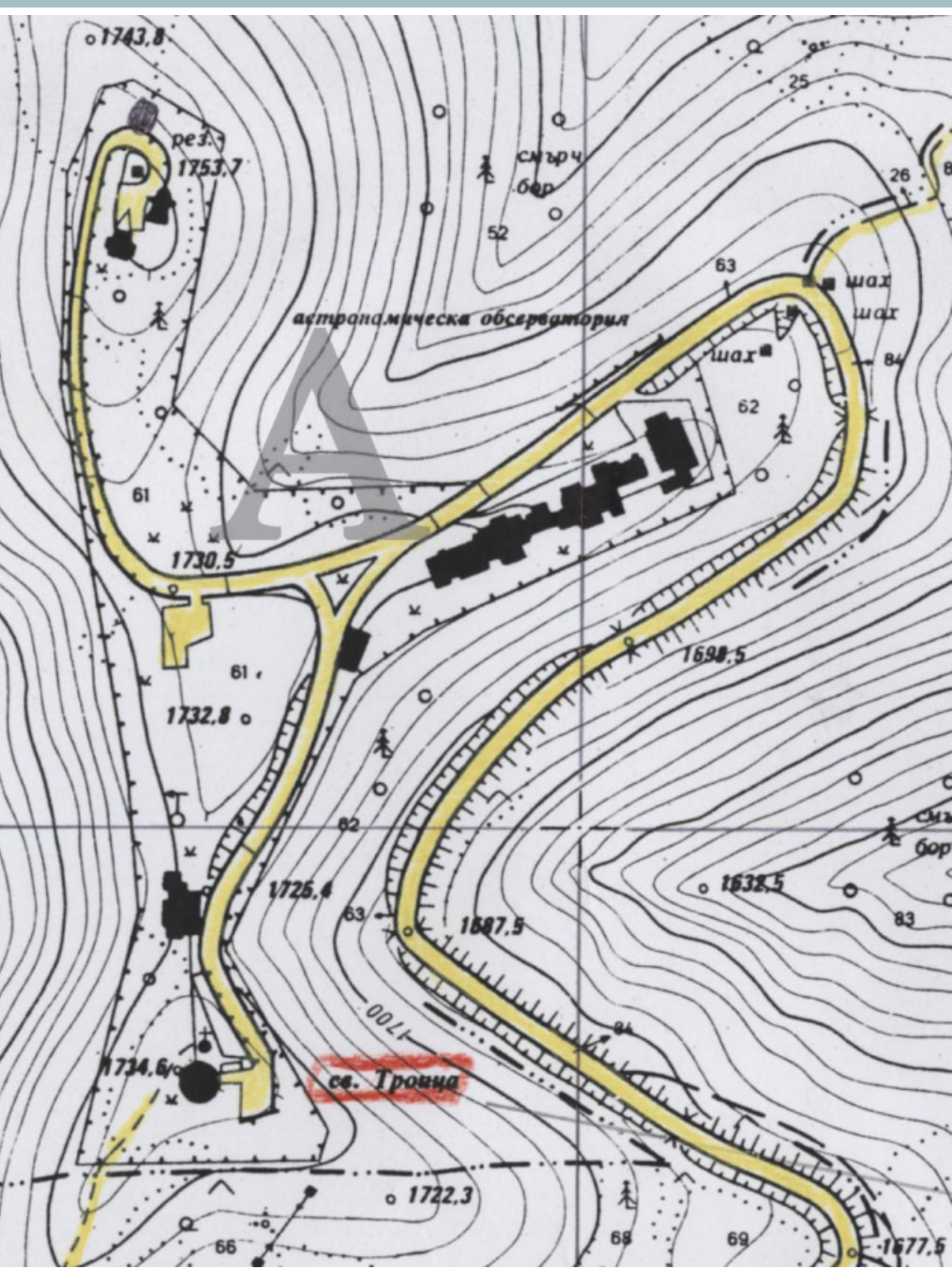
Galin Borisov

**Institute of astronomy and National astronomical
observatory, Bulgarian Academy of Sciences**

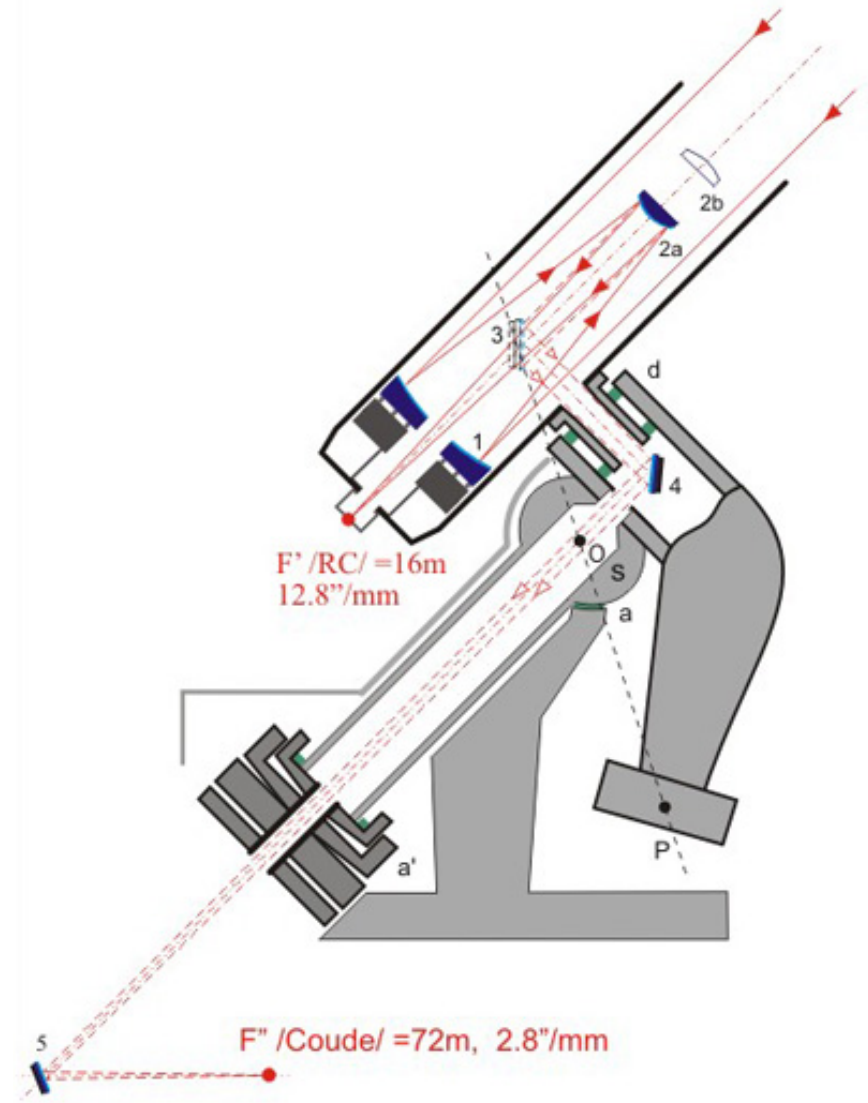
Where we are

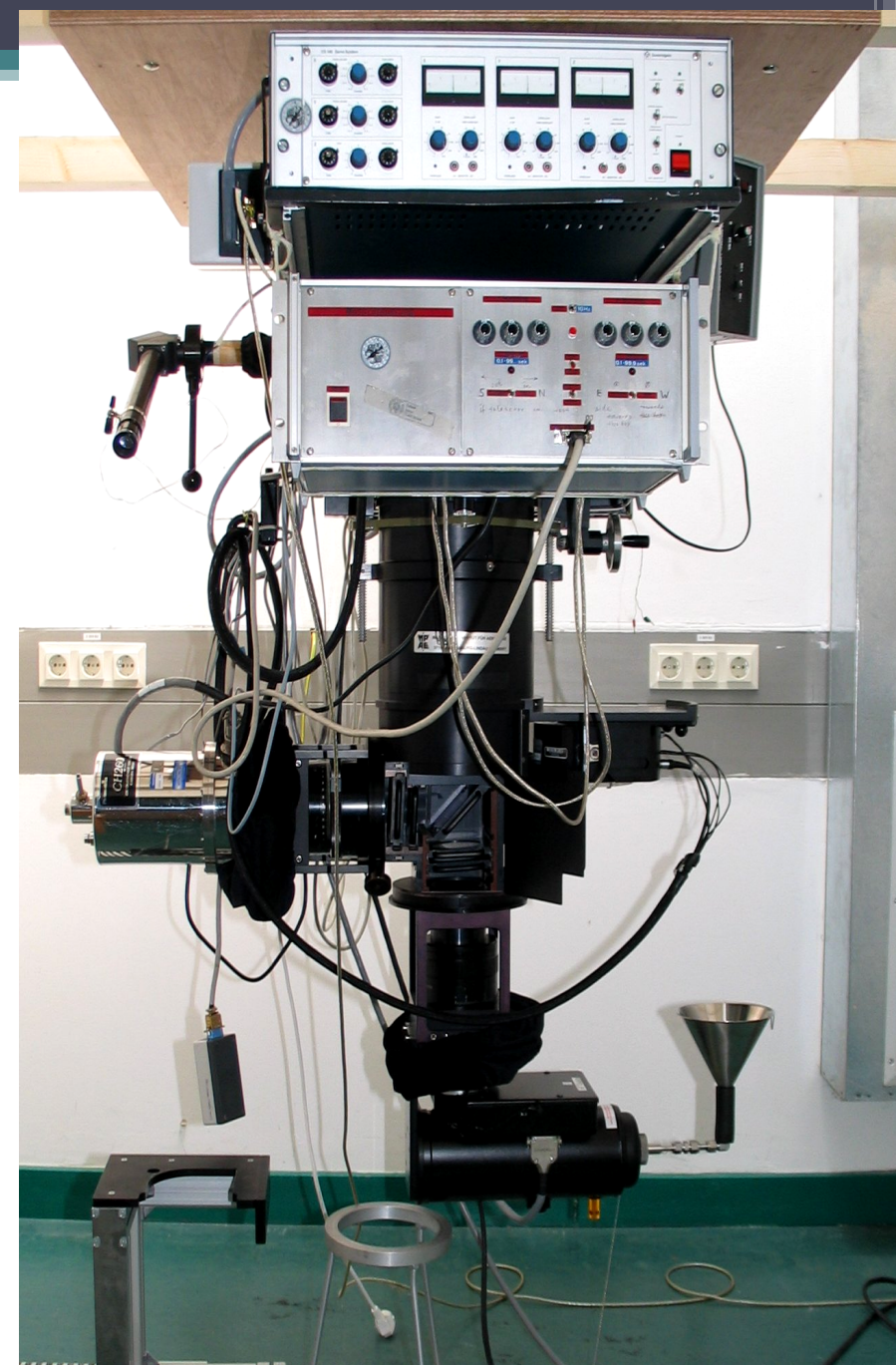
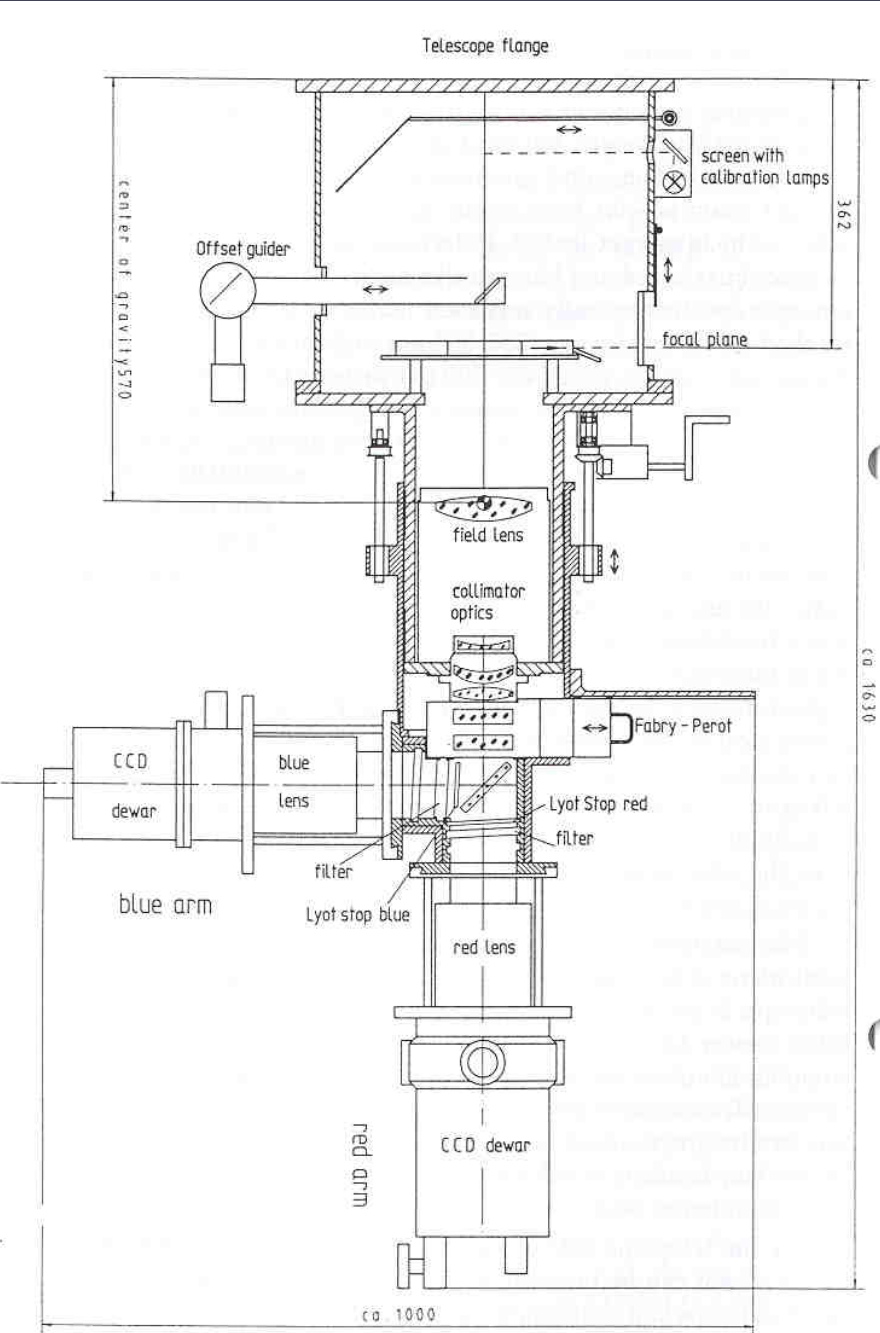
2-4m European Telescopes





2-m Ritchey-Chrétien-Coudé Telescope



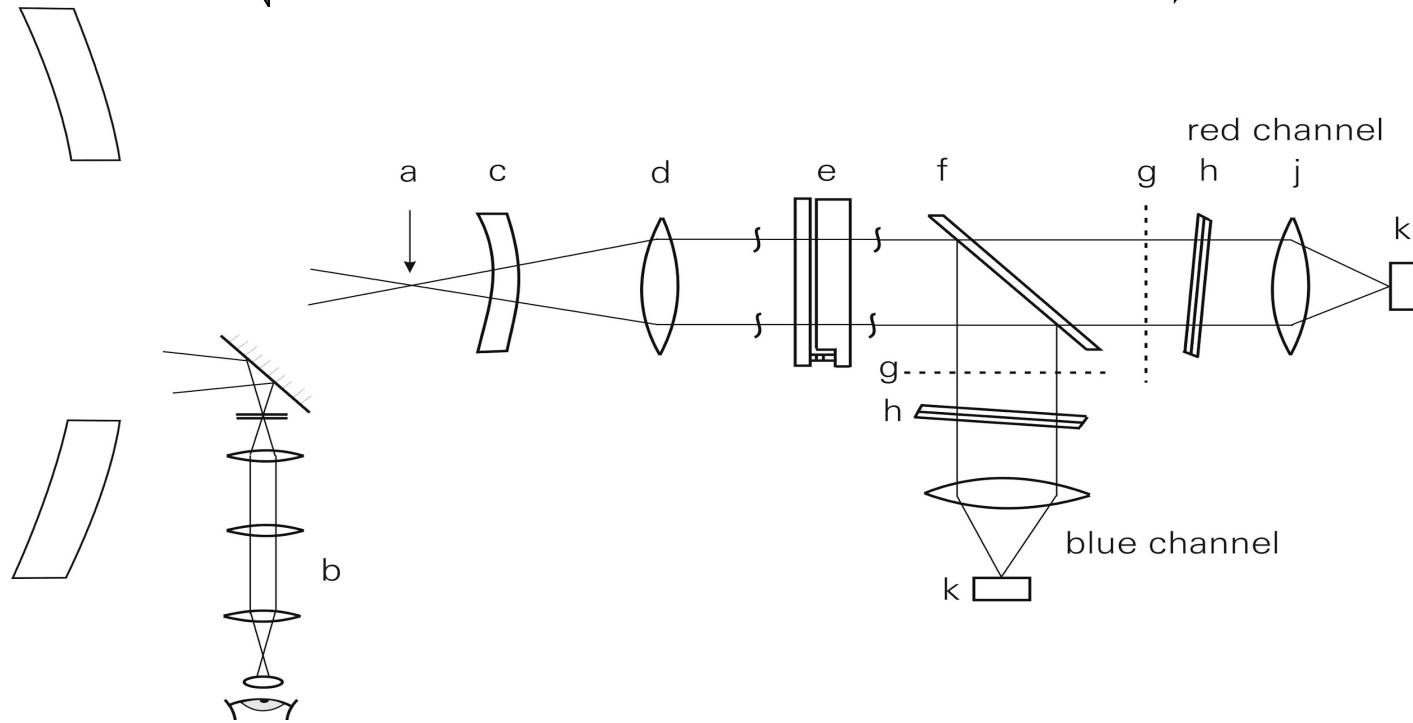


FoReRo2

16 m ← Focal length → 5.6 m

f/8 ← f ratio → f/2.8

0.17 arcsec/px ← Scale (1 px = 0.0135 mm) → 0.50 arcsec/px



FoReRo2: Modes of Observations

- Broadband imaging
- Narrowband imaging
- Long slit spectroscopy
- Fabry-Perot imaging
- **Imaging and spectro-polarimetry**



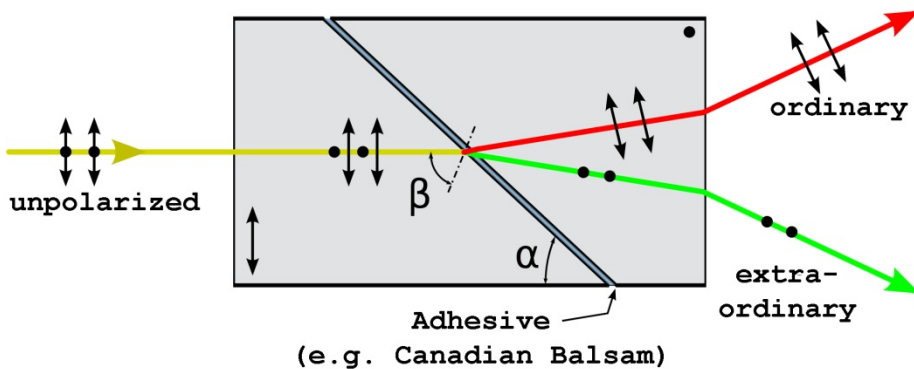


Ideal Polarimeter

Stokes vector $\mathbf{S}(I, Q, U, V)$

$$P = \frac{\sqrt{Q^2 + U^2}}{I} = \sqrt{\bar{Q}^2 + \bar{U}^2}, \text{ where } \bar{Q} = \frac{Q}{I}, \bar{U} = \frac{U}{I}$$

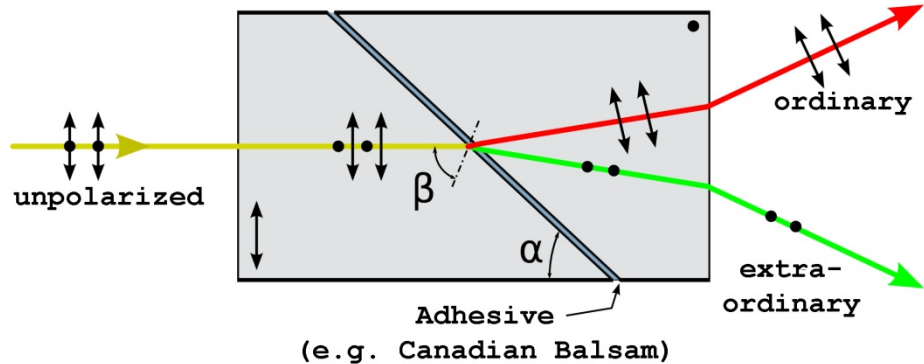
$$\theta = \frac{1}{2} \arctan \left(\frac{U}{\bar{Q}} \right)$$



$$Q = I_0 - I_{90}$$

$$U = I_{45} - I_{135}$$

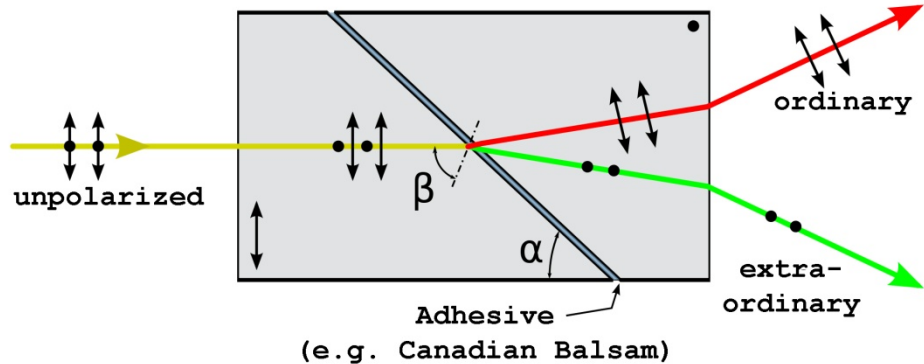
Real life polarimeter



$$F_{\parallel} = I + Q$$
$$F_{\perp} = I - Q$$

$$\frac{F_{\parallel} - F_{\perp}}{F_{\parallel} + F_{\perp}} = \frac{(I + Q) - (I - Q)}{(I + Q) + (I - Q)} = \frac{Q}{I}$$

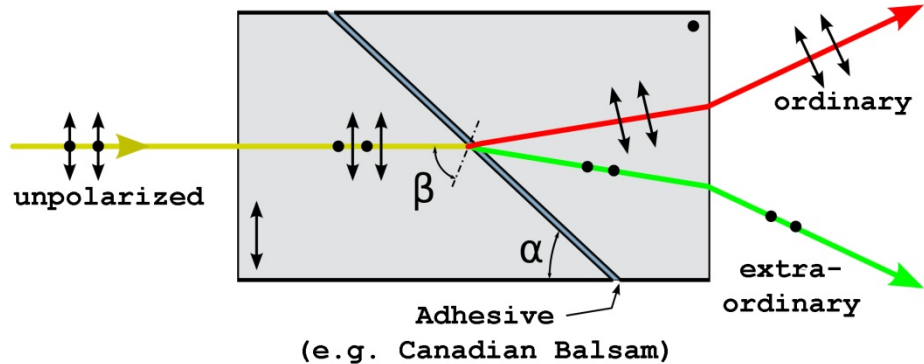
Real life polarimeter



$$F_{\parallel} = I + Q$$
$$F_{\perp} = I - Q$$

$$\frac{F_{\parallel} - F_{\perp}}{F_{\parallel} + F_{\perp}} = \frac{(I + Q) - (I - Q)}{(I + Q) + (I - Q)} = \frac{Q}{I}$$

Real life polarimeter



$$F_{\parallel} = I + Q$$
$$F_{\perp} = I - Q$$

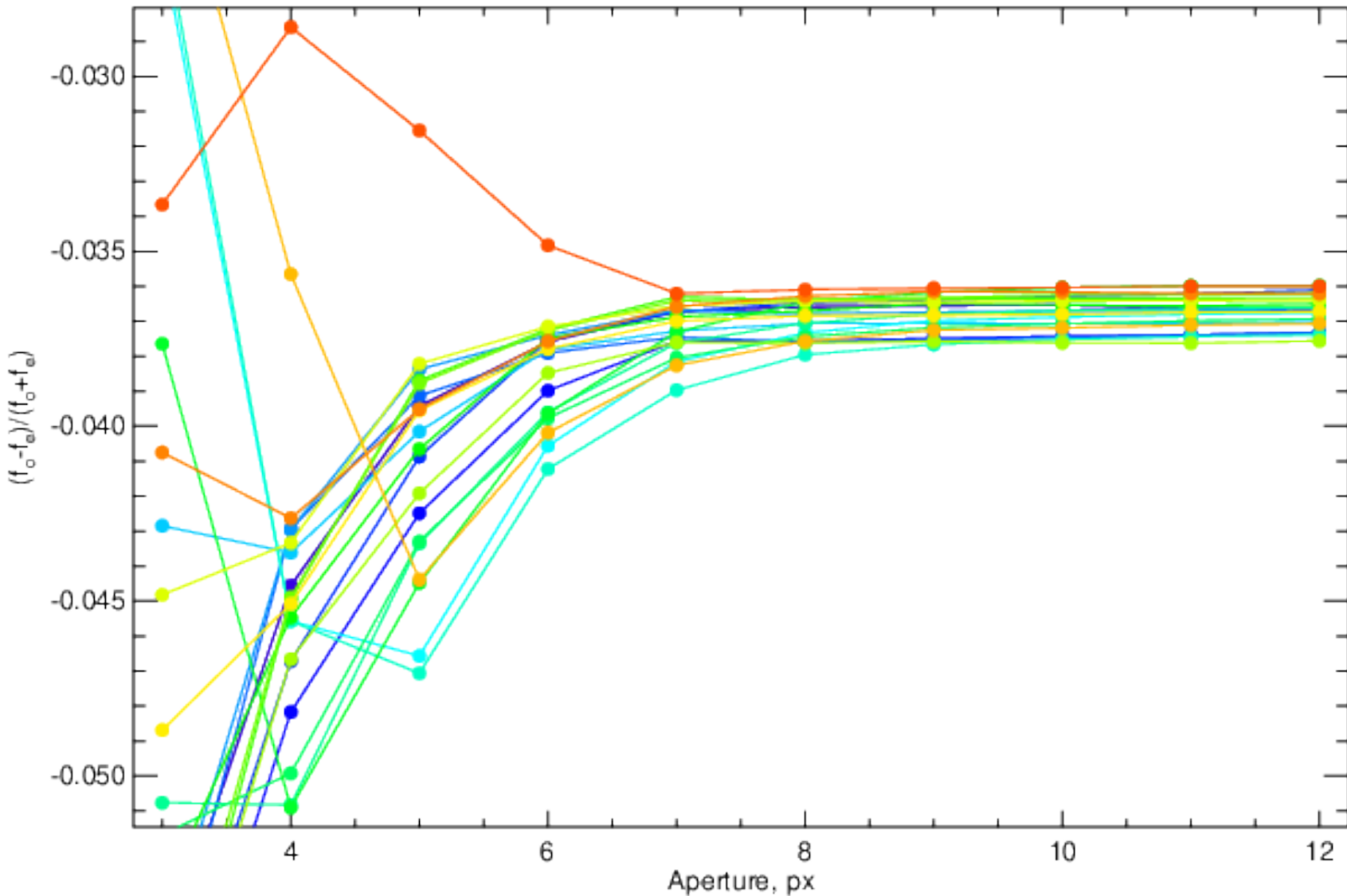
$$\frac{F_{\parallel} - F_{\perp}}{F_{\parallel} + F_{\perp}} = \frac{k_{\parallel}(I + Q) - k_{\perp}(I - Q)}{k_{\parallel}(I + Q) + k_{\perp}(I - Q)}$$

Polarimetry - Beam swaping

$$\frac{1}{2} \left[\left(\frac{f^{\parallel} - f^{\perp}}{f^{\parallel} + f^{\perp}} \right)_{0^\circ} - \left(\frac{f^{\parallel} - f^{\perp}}{f^{\parallel} + f^{\perp}} \right)_{90^\circ} \right] = \frac{1}{2} \left[\frac{k_{\parallel}(I+Q) - k_{\perp}(I-Q)}{k_{\parallel}(I+Q) + k_{\perp}(I-Q)} - \frac{k_{\parallel}(I-Q) - k_{\perp}(I+Q)}{k_{\parallel}(I-Q) + k_{\perp}(I+Q)} \right]$$

$$\frac{(k_{\parallel} + k_{\perp})^2 IQ - \overbrace{(k_{\parallel} - k_{\perp})^2 IQ}^0}{(k_{\parallel} + k_{\perp})^2 I^2 - \underbrace{(k_{\parallel} - k_{\perp})^2 Q^2}_0} = \frac{Q}{I}$$

Polarimetry - aperture choosing



Standard stars

Table 2: Results from imaging polarimetry of unpolarised and polarised standard stars.

Star	Date	Filter	P, %	σP , %	P_{cat} , %	σP_{cat} , %	$(P - P_{\text{cat}})$, %	$\sigma(P - P_{\text{cat}})$, %	Notes
Unpolarised standard stars									
HD42807	2014-12-20	V	0.0645	0.0108	0.0000	0.0000	0.0645	0.0108	UKIRT; 000...067
G191B2B	2017-12-15	R	0.1344	0.0538	0.0900	0.0480	0.0444	0.0721	NOT; 000...067
G191B2B	2017-12-15	R	0.1947	0.0864	0.0900	0.0480	0.1047	0.0989	NOT; 090...157
HD154892	2018-03-11	R	0.0661	0.0000	0.0500	0.0300	0.0161	0.0300	NOT; 000...067
HD154892	2018-03-11	R	0.1229	0.0000	0.0500	0.0300	0.0729	0.0300	NOT; 090...157
-	2018-10-02	R	0.0407	0.0276	0.0000	0.0000	0.0407	0.0276	000...067
G191B2B	2019-09-21	Rx	0.1277	0.0460	0.0900	0.0480	0.0377	0.0665	NOT; 000...067
G191B2B	2019-09-21	Rx	0.0861	0.0461	0.0900	0.0480	-0.0039	0.0666	NOT; 090...157
G191B2B	2019-10-21	Rx	0.1132	0.0495	0.0900	0.0480	0.0232	0.0689	NOT; 000...067
G191B2B	2019-10-21	Rx	0.1974	0.0504	0.0900	0.0480	0.1074	0.0696	NOT; 090...157
G191B2B	2019-10-22	Rx	0.0336	0.0472	0.0900	0.0480	-0.0564	0.0673	NOT; 000...067
G191B2B	2019-10-22	Rx	0.0861	0.0459	0.0900	0.0480	-0.0039	0.0664	NOT; 090...157
G191B2B	2019-10-24	Rx	0.1046	0.0623	0.0900	0.0480	0.0146	0.0787	NOT; 000...067
G191B2B	2019-10-24	Rx	0.0623	0.0628	0.0900	0.0480	-0.0277	0.0790	NOT; 090...157
G191B2B	2019-10-25	Rx	0.0896	0.0739	0.0900	0.0480	-0.0004	0.0881	NOT; 000...067
G191B2B	2019-10-25	Rx	0.0627	0.0763	0.0900	0.0480	-0.0273	0.0901	NOT; 090...157
G191B2B	2020-04-18	Rx	0.0966	0.0545	0.0900	0.0480	0.0066	0.0727	NOT; 000...067
G191B2B	2020-04-18	Rx	0.1165	0.0552	0.0900	0.0480	0.0265	0.0731	NOT; 090...157
G191B2B	2020-04-25	Rx	0.0474	0.0540	0.0900	0.0480	-0.0426	0.0722	NOT; 000...067
G191B2B	2020-04-25	Rx	0.0355	0.0544	0.0900	0.0480	-0.0545	0.0725	NOT; 090...157
HD154892	2020-04-30	Rx	0.0780	0.0346	0.0500	0.0300	0.0280	0.0458	NOT; 000...067
HD154892	2020-04-30	Rx	0.0532	0.0347	0.0500	0.0300	0.0032	0.0459	NOT; 090...157

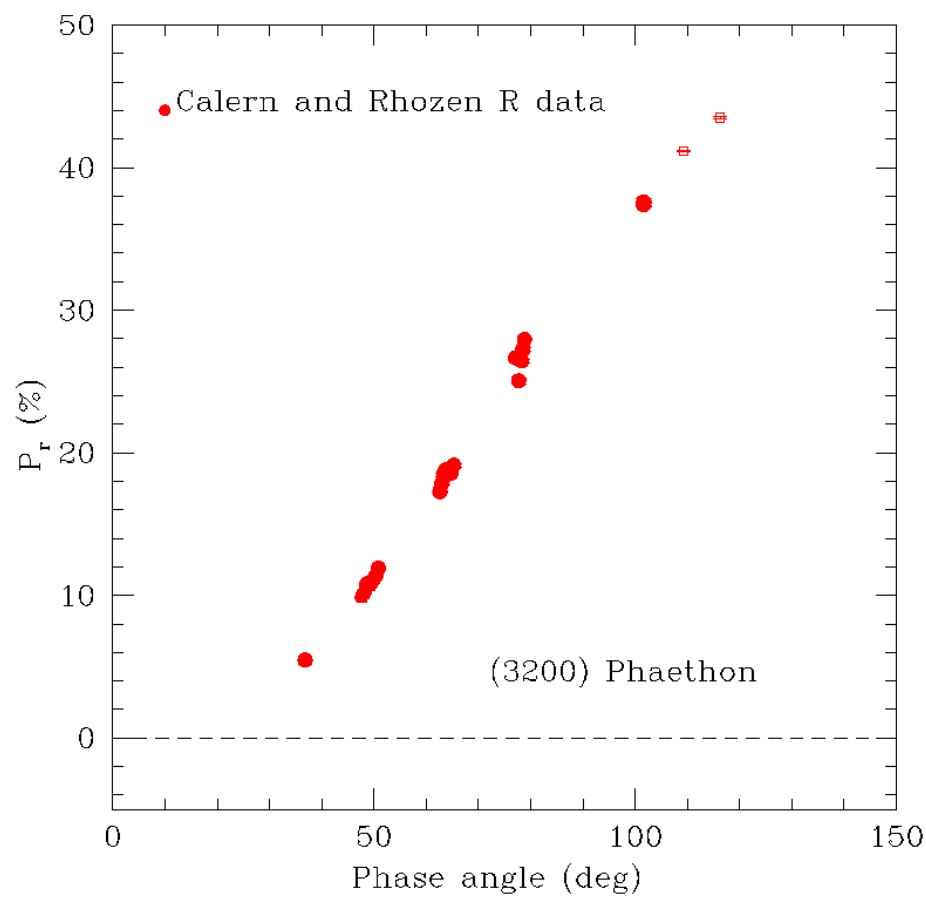
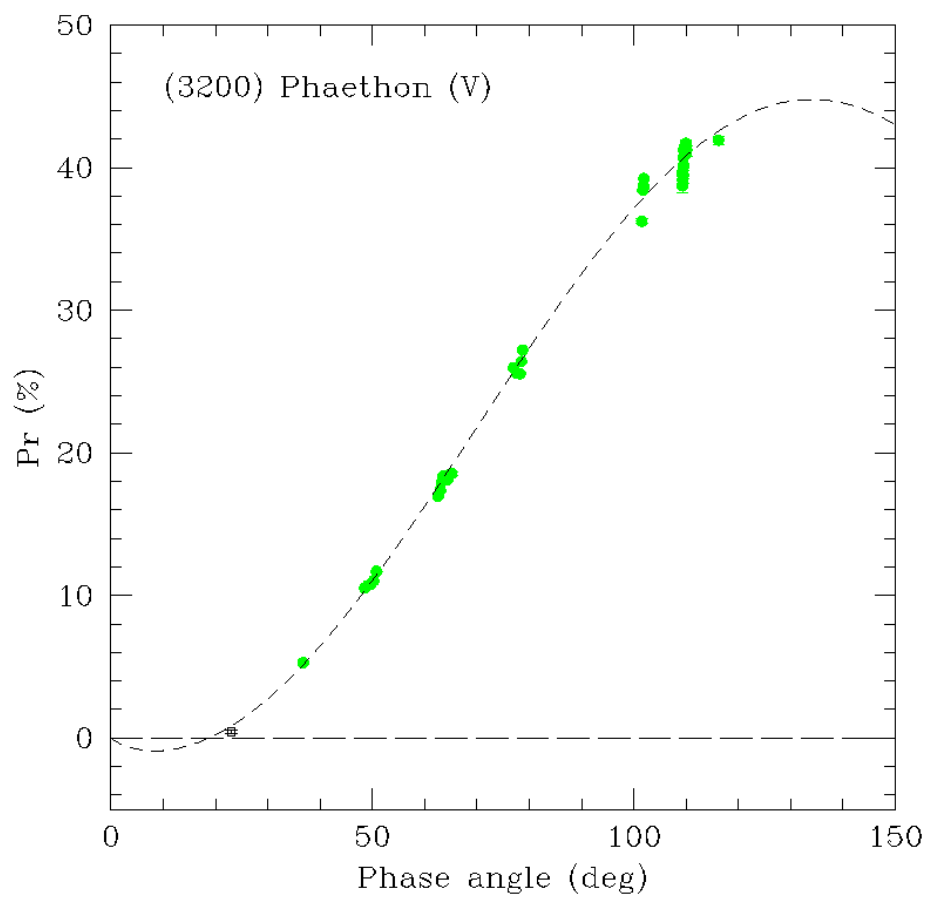
Standard stars

Table 2: Results from imaging polarimetry of unpolarised and polarised standard stars.

Star	Date	Filter	P, %	σP , %	P_{cat} , %	σP_{cat} , %	$(P - P_{\text{cat}})$, %	$\sigma(P - P_{\text{cat}})$, %	Notes
Polarised standard stars									
HD183143	2014-12-20	IF890	4.5545	0.0576	4.7199	–	-0.1655	0.0576	UKIRT; 000...067
HD183143	2014-12-20	IF890	4.5485	0.0579	4.7199	–	-0.1714	0.0579	UKIRT; 090...157
HD43384	2015-03-18	IF890	2.2991	0.0205	2.2149	–	0.0843	0.0205	UKIRT; 000...067
HD183143	2015-03-21	IF890	4.6824	0.0417	4.7199	–	-0.0375	0.0417	UKIRT; 000...067
HD183143	2015-04-23	IF890	4.5545	0.0576	4.7199	–	-0.1655	0.0576	UKIRT; 000...067
HD183143	2015-04-23	IF890	4.5485	0.0579	4.7199	–	-0.1714	0.0579	UKIRT; 090...157
HD183143	2015-04-26	IF890	4.5545	0.0576	4.7199	–	-0.1655	0.0576	UKIRT; 000...067
HD183143	2015-04-26	IF890	4.5485	0.0579	4.7199	–	-0.1714	0.0579	UKIRT; 090...157
BDp59389	2017-12-15	R	6.4672	0.0220	6.4300	0.0220	0.0372	0.0311	NOT; 000...067
BDp59389	2017-12-15	R	6.9850	0.0219	6.4300	0.0220	0.5550	0.0310	NOT; 090...157
HD161056	2018-03-11	R	3.8850	0.0349	4.0120	0.0320	-0.1270	0.0473	NOT; 000...067
HD161056	2018-03-11	R	3.7389	0.0304	4.0120	0.0320	-0.2731	0.0442	NOT; 090...157
BDp59389	2019-10-25	Rx	6.3438	0.0425	6.4300	0.0220	-0.0862	0.0479	NOT; 000...067
BDp59389	2019-10-25	Rx	6.2468	0.0429	6.4300	0.0220	-0.1832	0.0482	NOT; 090...157
HD25443	2020-04-18	Rx	4.7103	0.0352	4.7340	0.0450	-0.0237	0.0571	NOT; 000...067
HD25443	2020-04-18	Rx	4.6662	0.0351	4.7340	0.0450	-0.0678	0.0571	NOT; 090...157
HD25443	2020-04-25	Rx	4.6661	0.0292	4.7340	0.0450	-0.0679	0.0536	NOT; 000...067
HD25443	2020-04-25	Rx	4.6914	0.0292	4.7340	0.0450	-0.0426	0.0536	NOT; 090...157
HD161056	2020-04-30	Rx	3.9059	0.0339	4.0120	0.0320	-0.1061	0.0467	NOT; 000...067
HD161056	2020-04-30	Rx	3.8460	0.0340	4.0120	0.0320	-0.1660	0.0467	NOT; 090...157

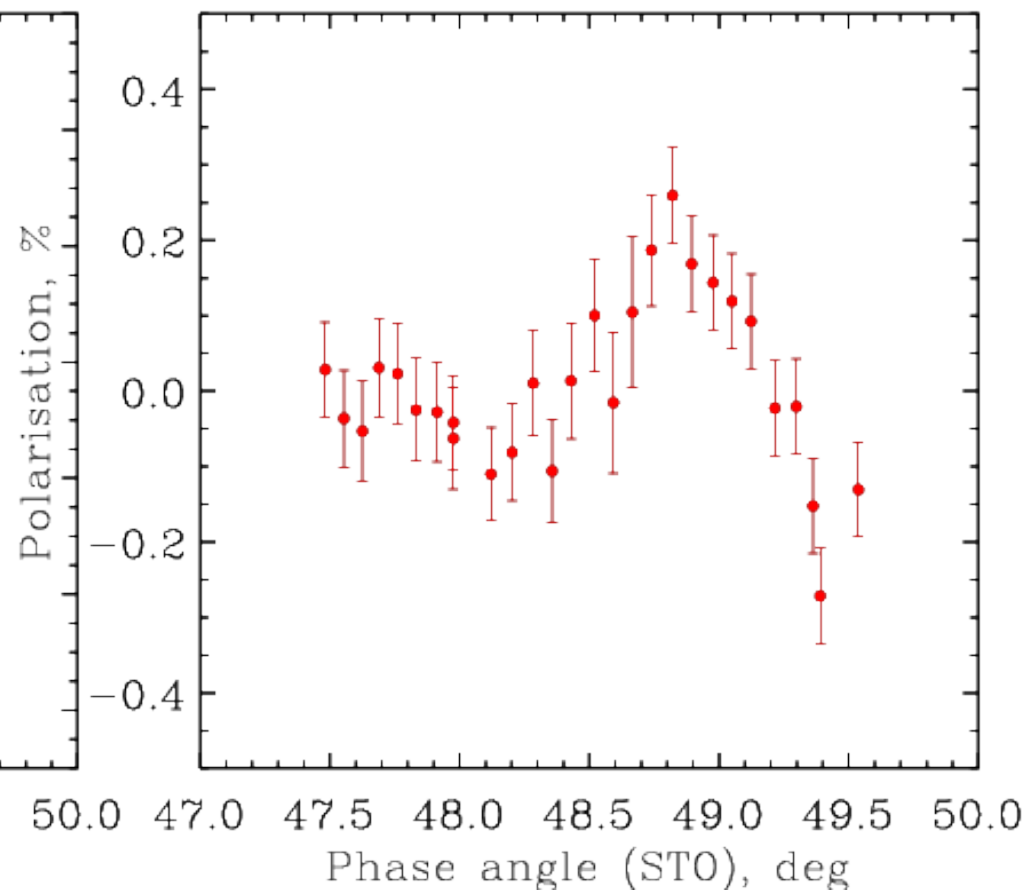
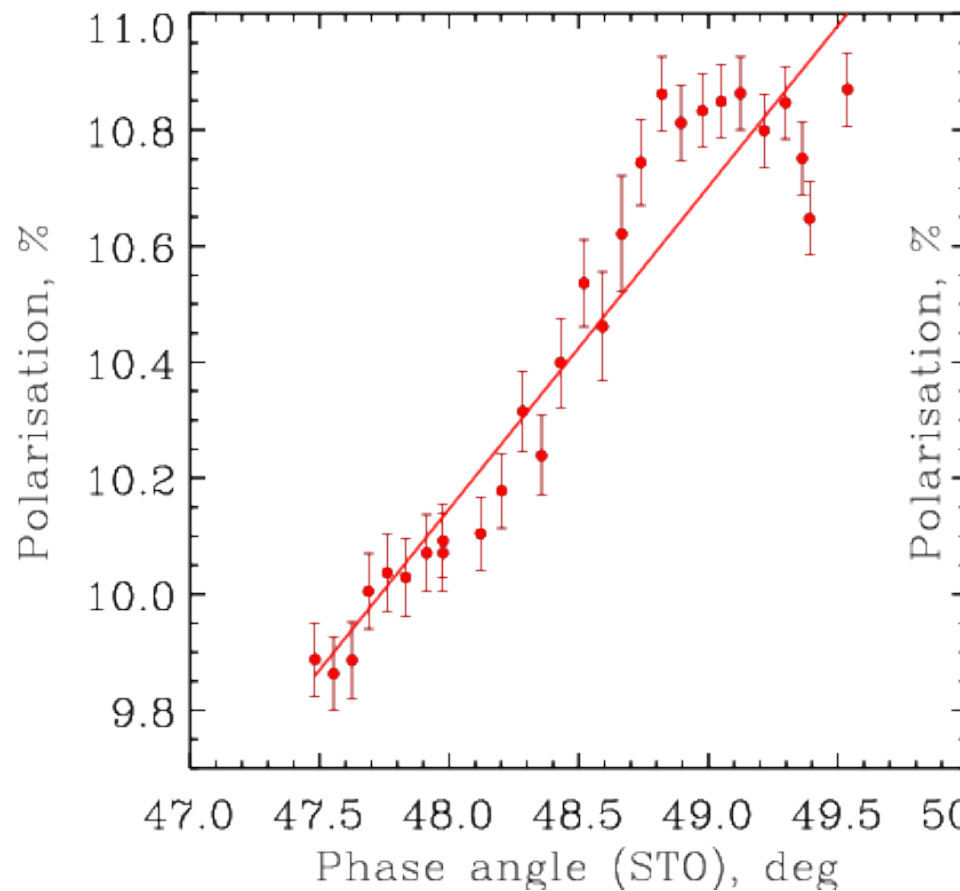
Polarimetry of (3200) Phaeton

Devogèle, M., et al., MNRAS 479, 3498–3508 (2018)

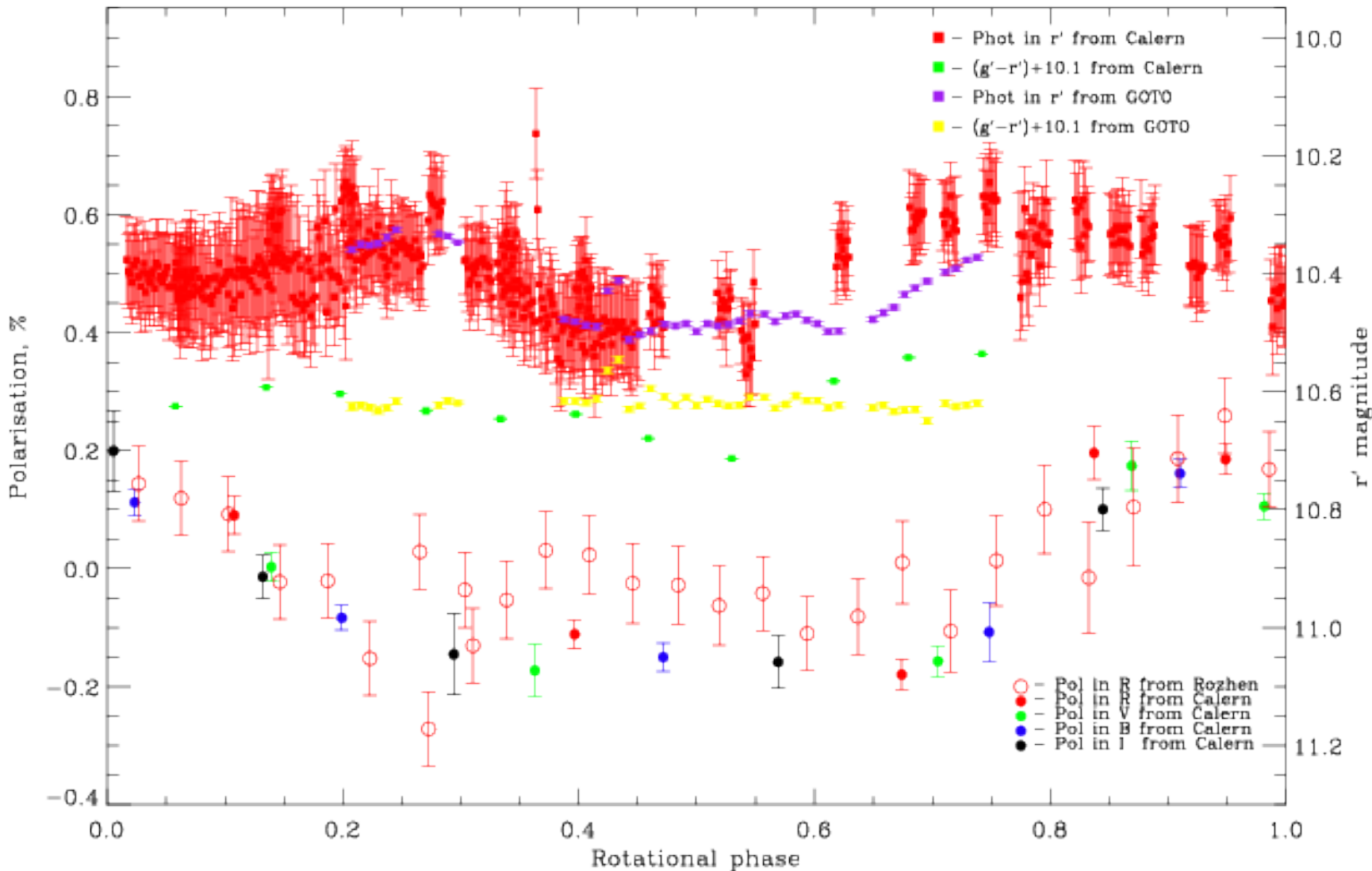


Polarimetry of (3200) Phaeton

Borisov, G. et al., MNRAS 480, L131–L135 (2018)



Polarimetry of (3200) Phaeton



Polarimetry of (3200) Phaeton

Taylor P. A., et al., 2018, 49th Lunar and Planetary Science Conference, The Woodlands, Texas, USA, LPI Contribution No. 2083, 2509

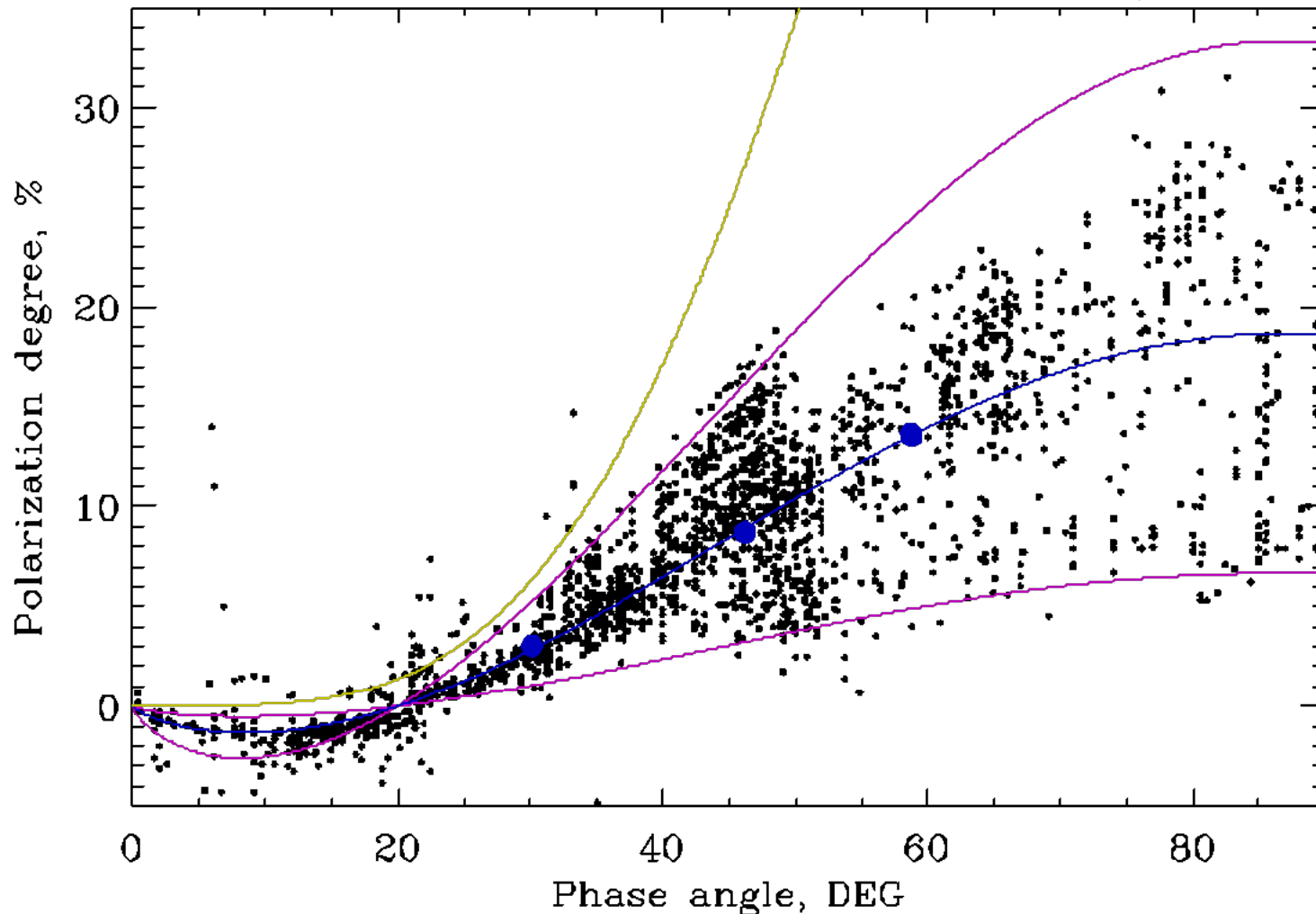
Surface features are subtle at the 75-meter resolution of the Arecibo radar images, barring two prominent features: a concavity near the equator and a radar dark feature near one of the poles. Figure 1 shows the dark feature that may be a polar crater or a relatively flat region compared to the local topography.



Figure 1. Arecibo radar image of 3200 Phaethon with 75-meter resolution. The echo is rather non-descript, though there is a prominent radar dark feature (circled in red) near one of the poles.

Polarimetry of the dust in the comet 103P/Hartley 2

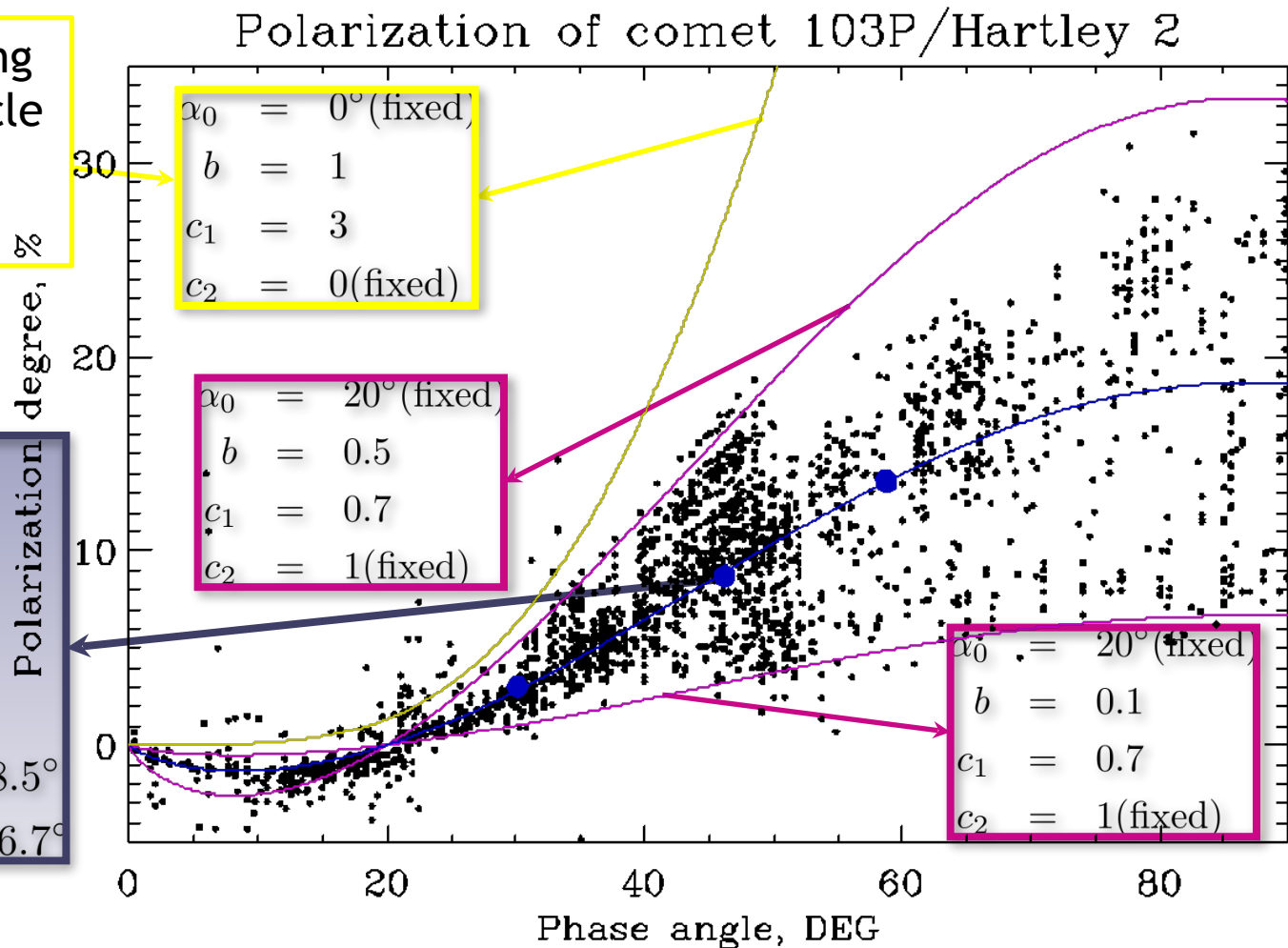
Polarization of comet 103P/Hartley 2



Rayleigh scattering
from single particle
with $P_{\max}=1$ at
 $\alpha=90^\circ$

Results

α_0	=	20° (fixed)
b	=	0.28
c_1	=	0.745
c_2	=	1(fixed)
s	=	0.12375
P_{\min}	=	$-1.33\% \rightarrow \alpha = 8.5^\circ$
P_{\max}	=	$18.65\% \rightarrow \alpha = 86.7^\circ$



$$P(\alpha) = b (\sin \alpha)^{c_1} \left(\cos \frac{\alpha}{2} \right)^{c_2} \sin (\alpha - \alpha_0)$$

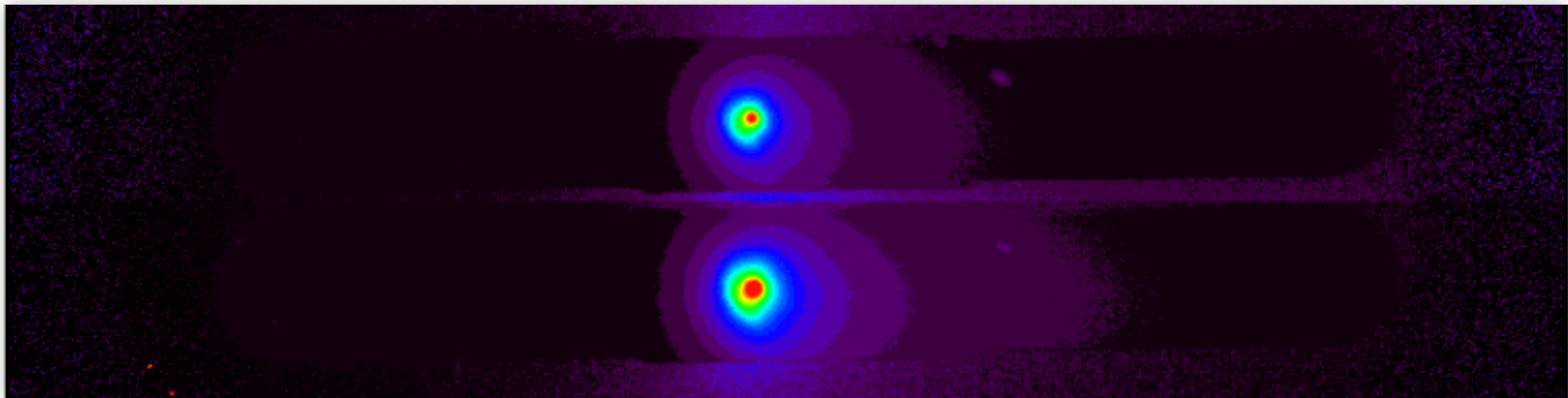
$$s = b (\sin \alpha_0)^{c_1} \left(\cos \frac{\alpha_0}{2} \right)^{c_2}$$

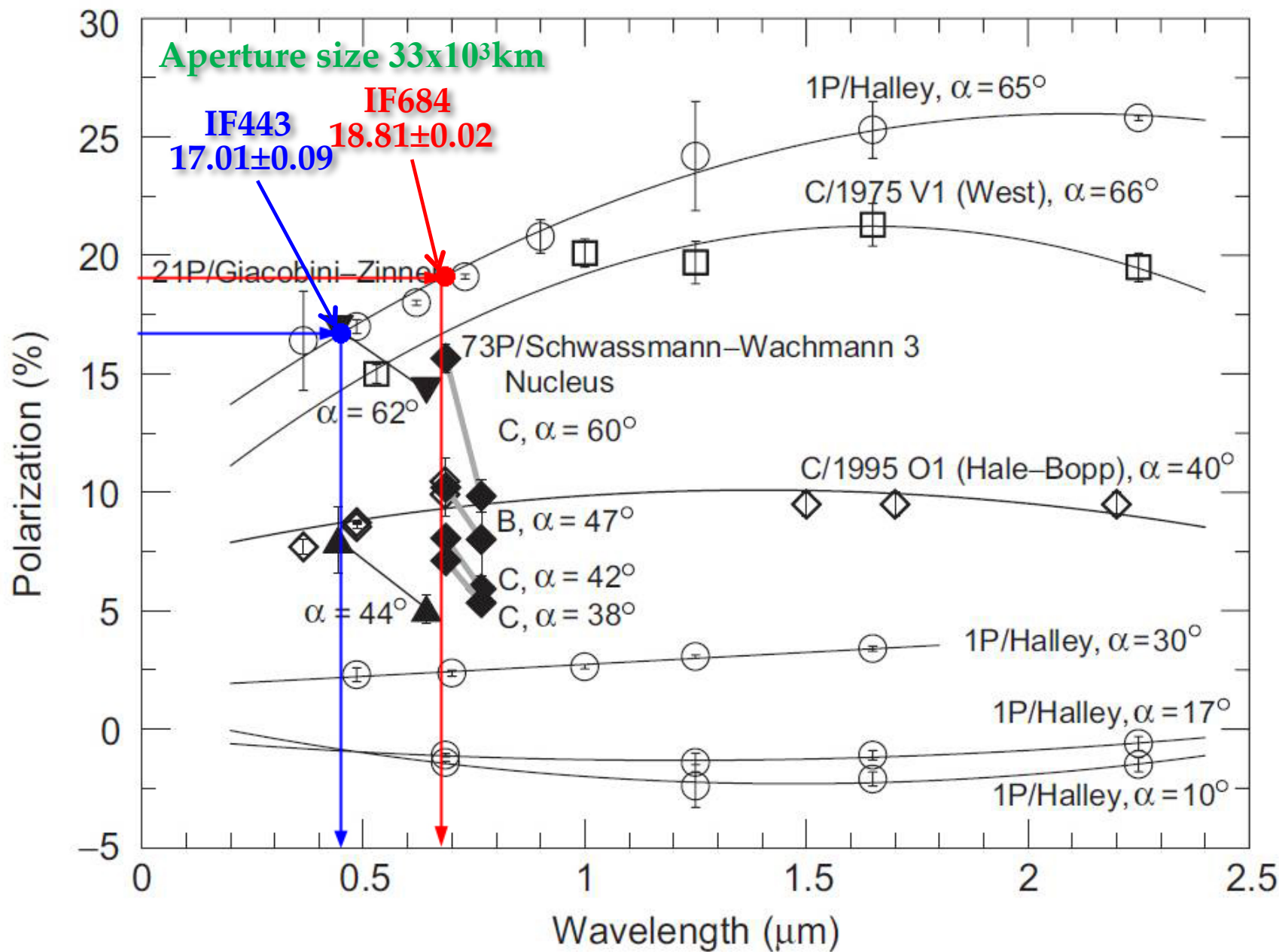
Polarimetry and spectropolarimetry of comet C/2013 R1 (LoveJoy)

Date	r, AU	Δ , AU	Phase, °	Obs. mode
20 Dec 2013	0.8132	0.8562	72.2	High resolution spectroscopy
21 Dec 2013	0.8123	0.8765	71.1	High resolution spectroscopy
22 Dec 2013	0.8118	0.8965	70.1	High resolution spectroscopy
23 Dec 2013	0.8118	0.9161	69.1	High resolution spectroscopy
24 Dec 2013	0.8122	0.9355	68.1	High resolution spectroscopy
29 Dec 2013	0.8210	1.0305	63.0	Imaging polarimetry
30 Dec 2013	0.8240	1.0495	62.0	Gas and dust coma imaging
31 Dec 2013	0.8275	1.0675	61.0	H_2O^+ tail imaging
03 Jan 2014	0.8405	1.1205	58.1	Spectro-polarimetry
04 Jan 2014	0.8455	1.1375	57.2	Spectro-polarimetry
08 Jan 2014	0.8631	1.1865	54.6	Gas, dust & H_2O^+ tail imaging

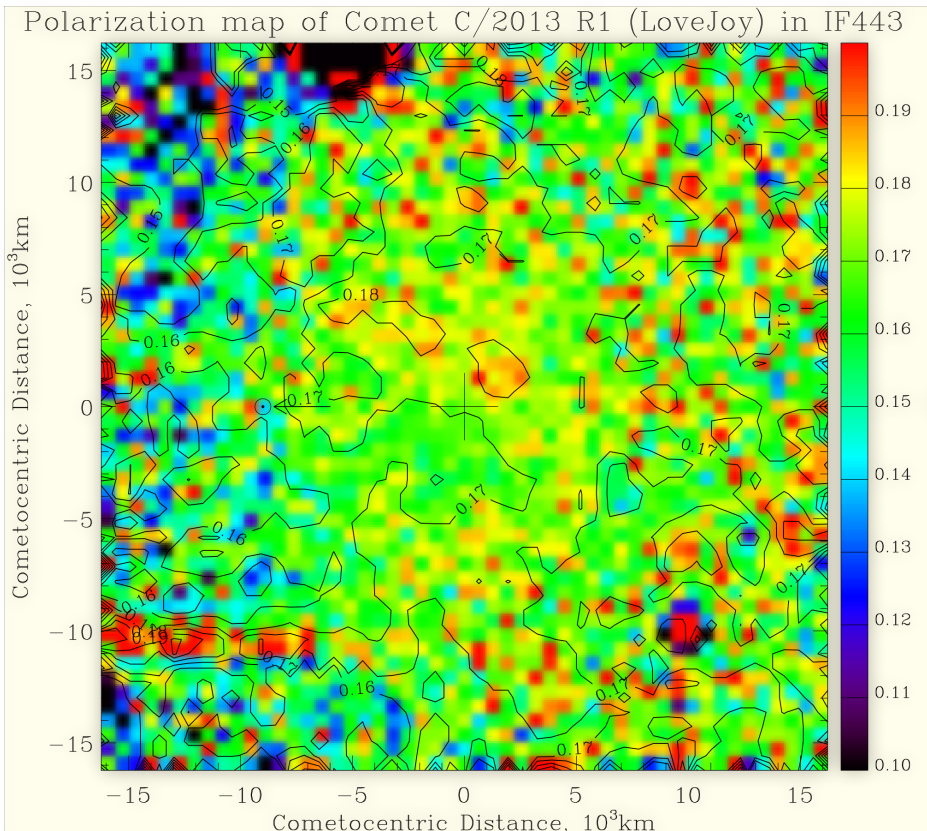
Polarimetry and spectropolarimetry of comet C/2013 R1 (LoveJoy)

- Imaging polarimetry
 - Wollaston prism
 - Dichroic beam splitter
 - Blue continuum (BC) at 443 nm – filter IF443
 - Red continuum (RC) at 684 nm – filter IF684
 - Beam swapping technique

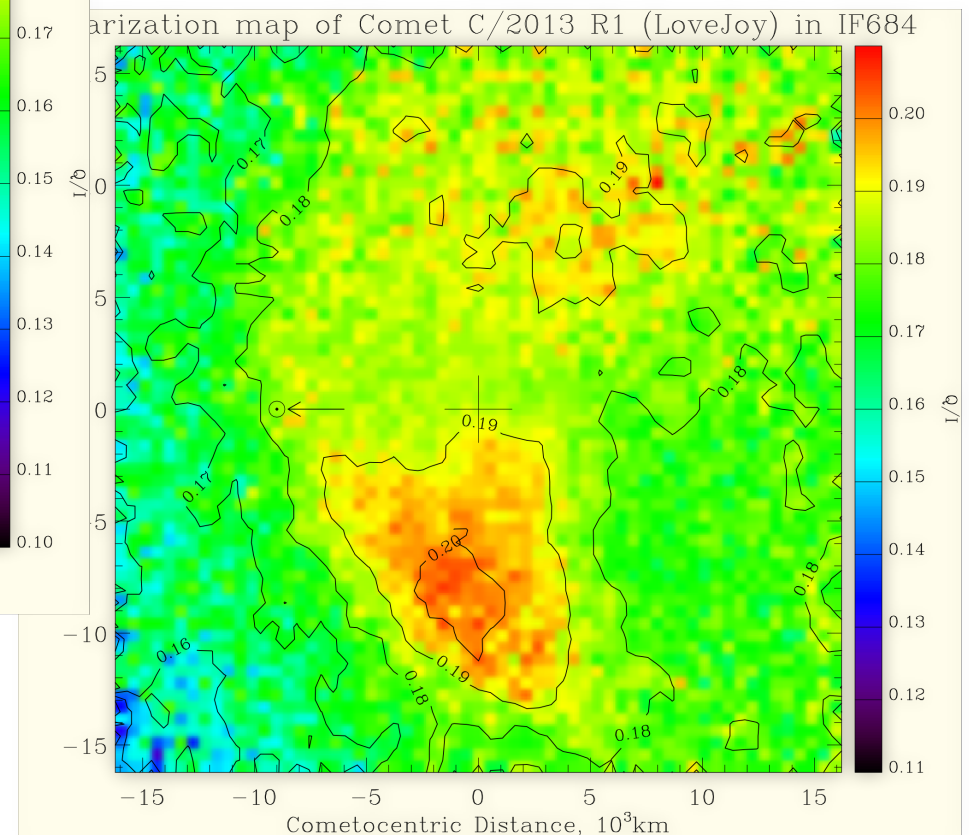




Polarimetry and spectropolarimetry of comet C/2013 R1 (LoveJoy)

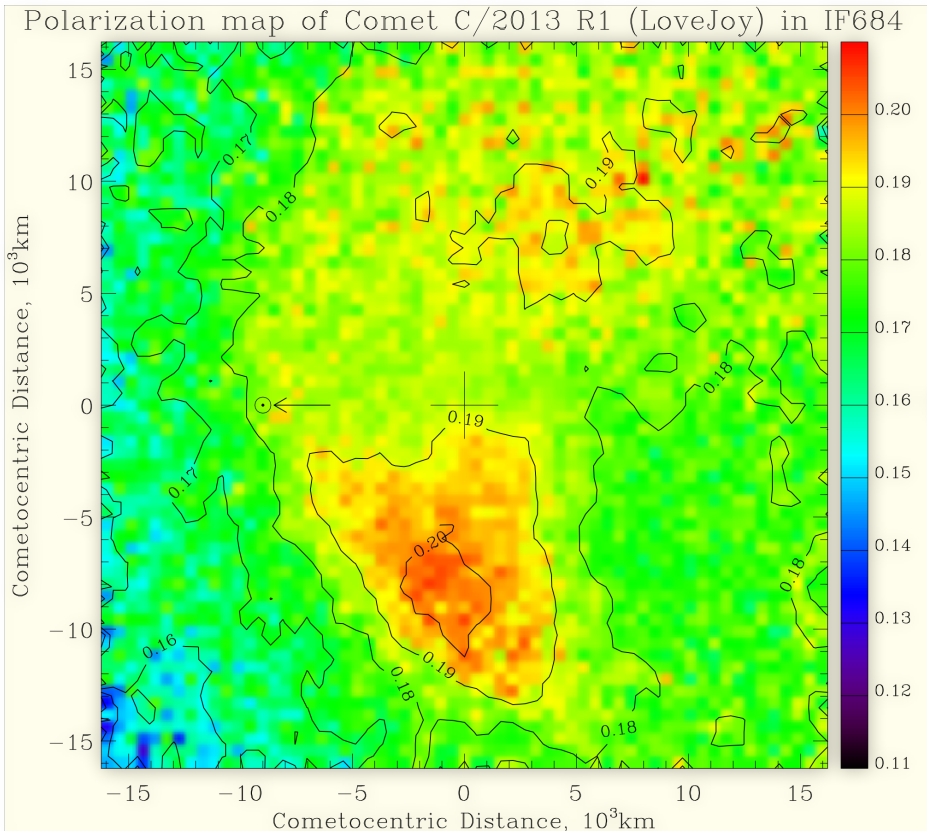


BC: IF 443nm

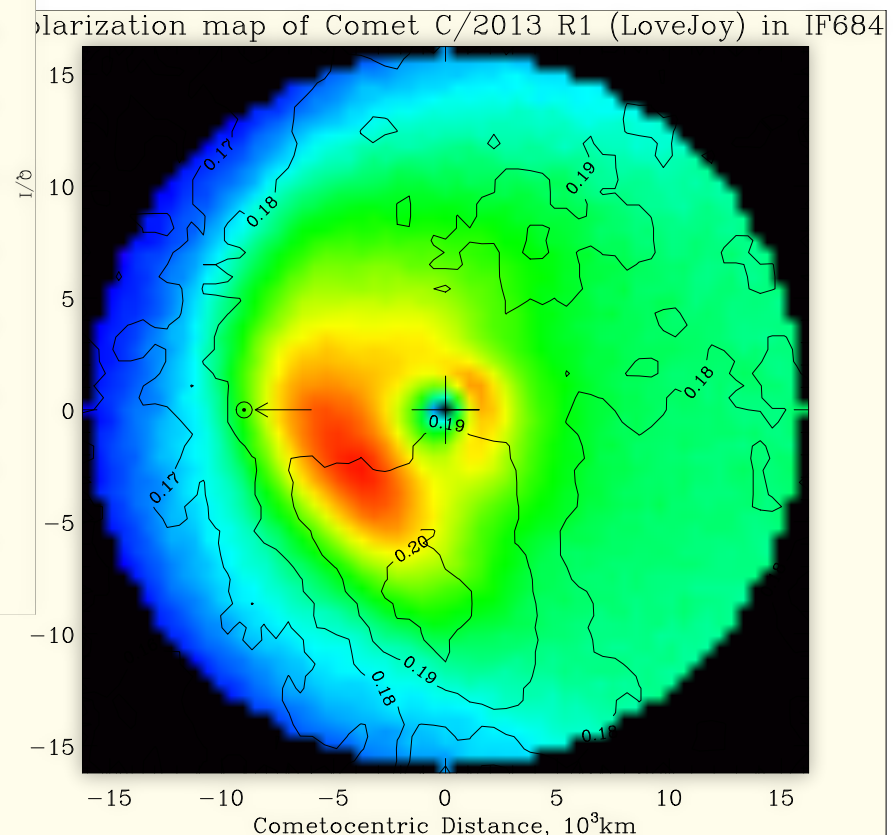


RC: IF 684nm

Polarimetry and spectropolarimetry of comet C/2013 R1 (LoveJoy)

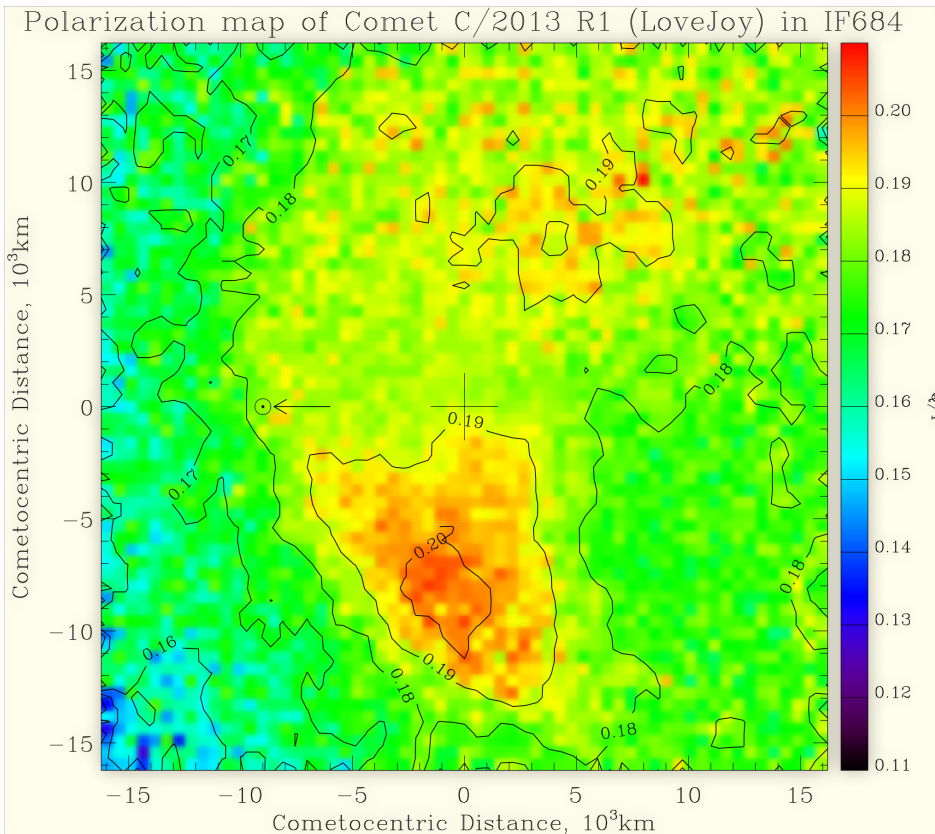


RC: IF 684nm

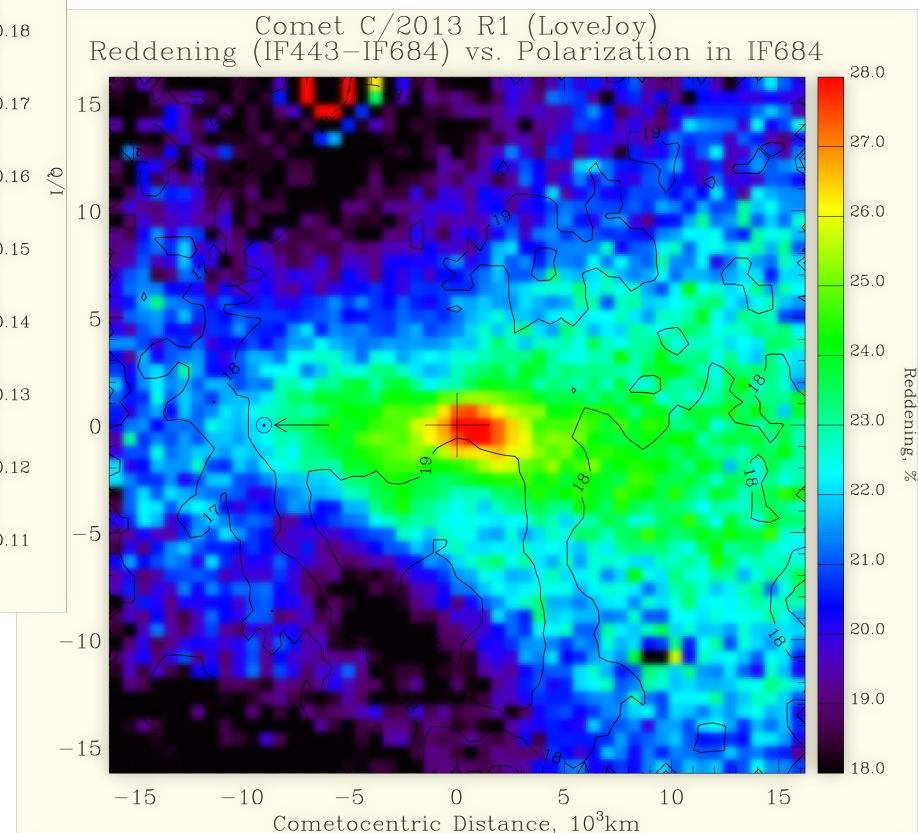


Enhanced dust
coma structures

Polarimetry and spectropolarimetry of comet C/2013 R1 (LoveJoy)



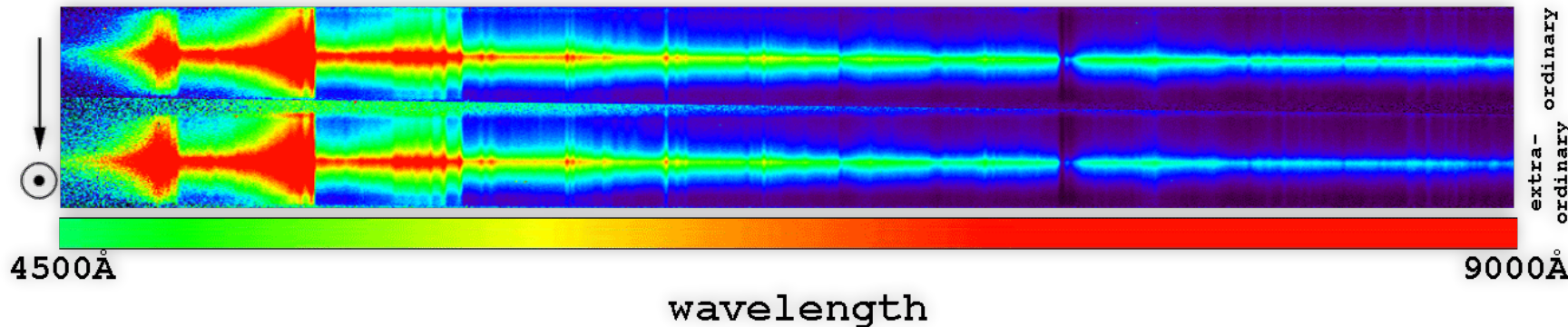
RC: IF 684nm



Dust reddening
Color map

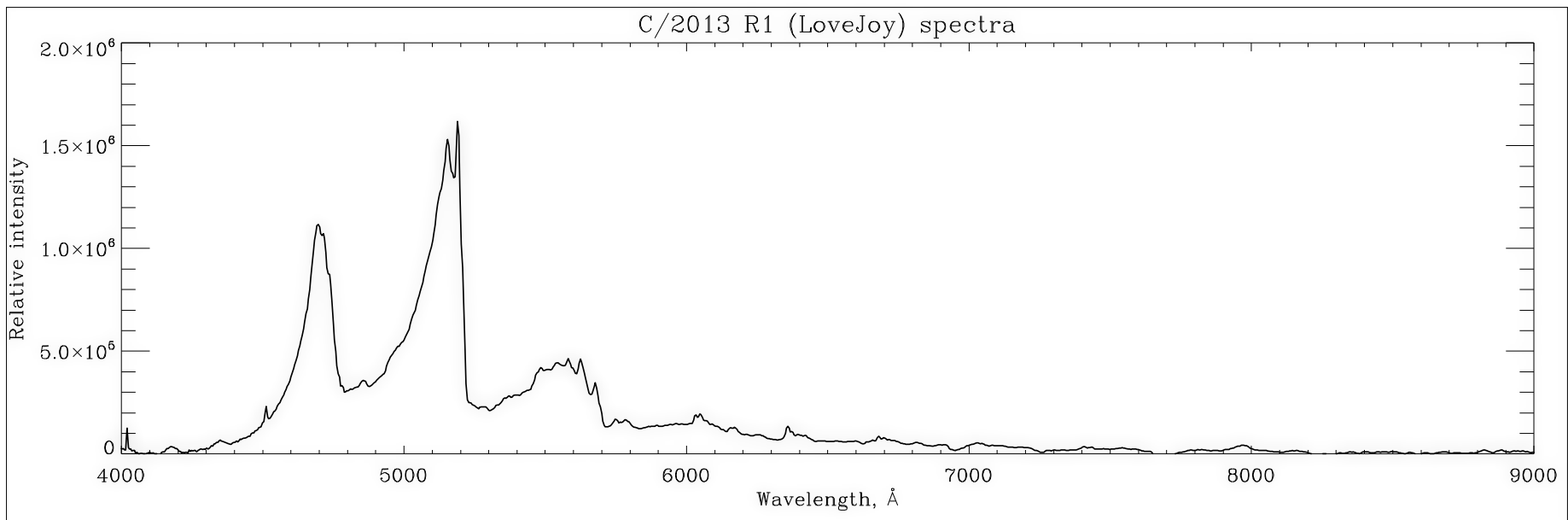
Polarimetry and spectropolarimetry of comet C/2013 R1 (LoveJoy)

- Spectro polarimetry
 - Long slit & Grism 300 lines / mm
 - Wavelength coverage – 450 – 900 nm
 - Beam swapping technique

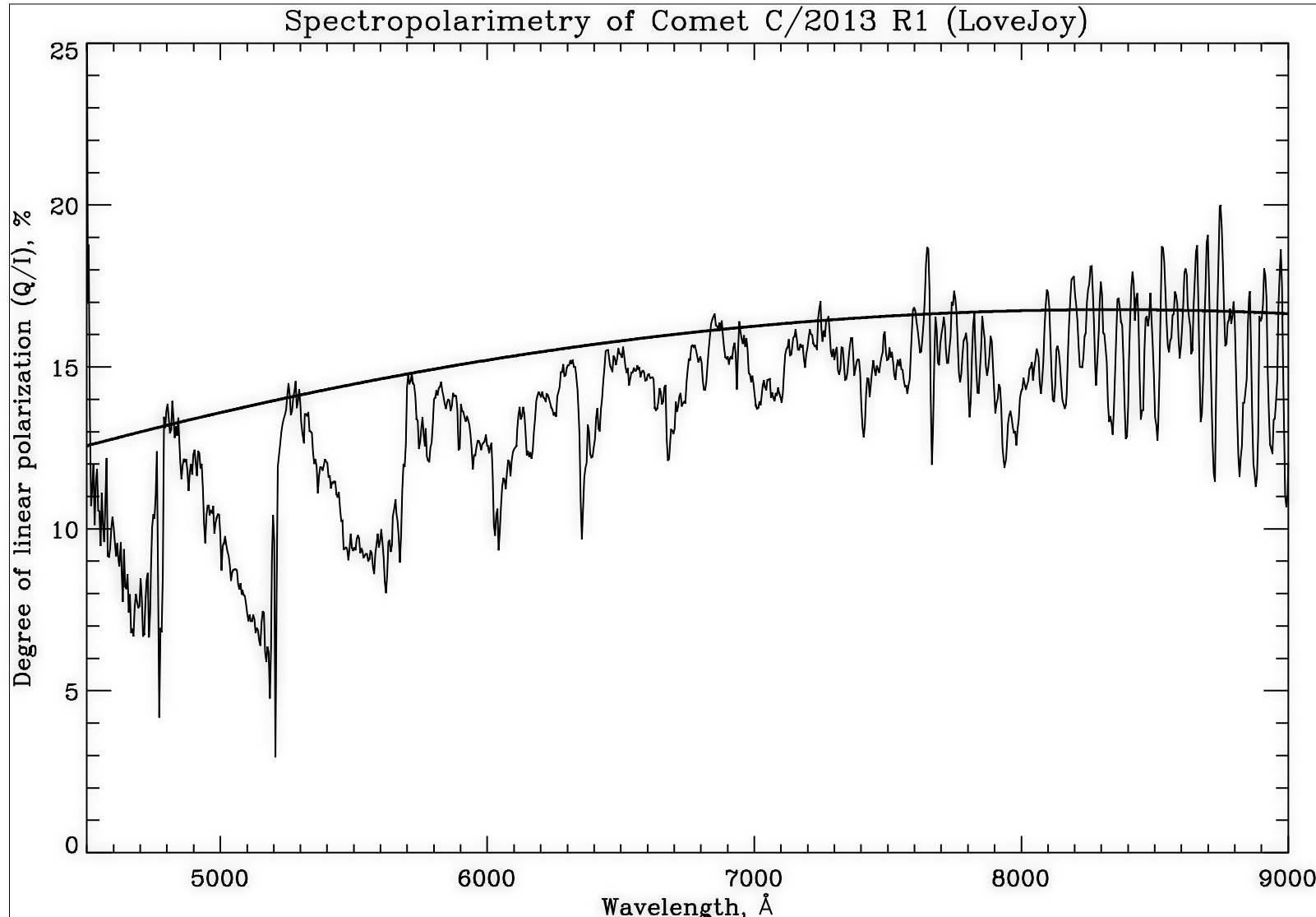


Polarimetry and spectropolarimetry of comet C/2013 R1 (LoveJoy)

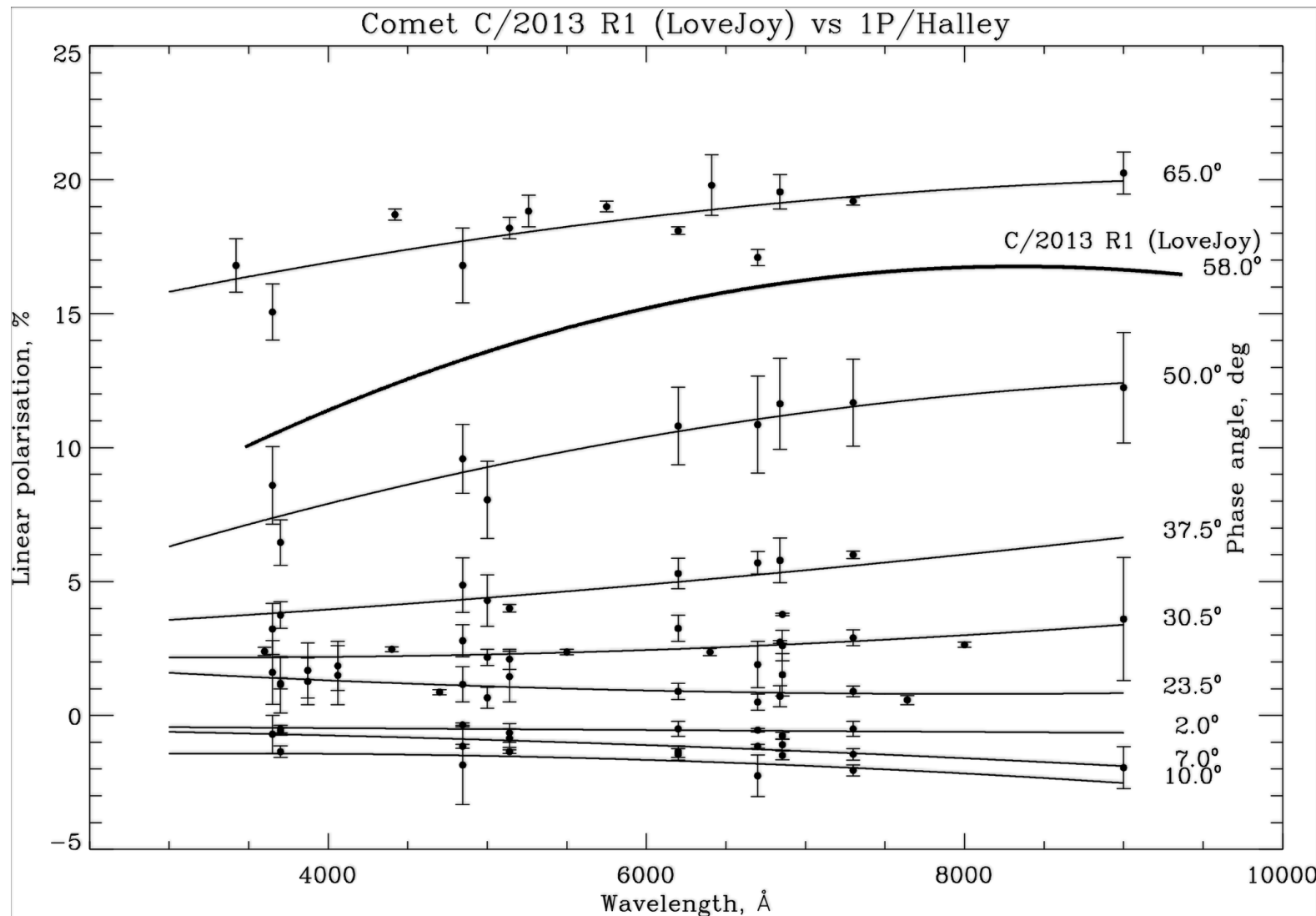
- Spectro polarimetry
 - Long slit & Grism 300 lines/mm
 - Wavelength coverage – 450 – 900 nm
 - Beam swapping technique



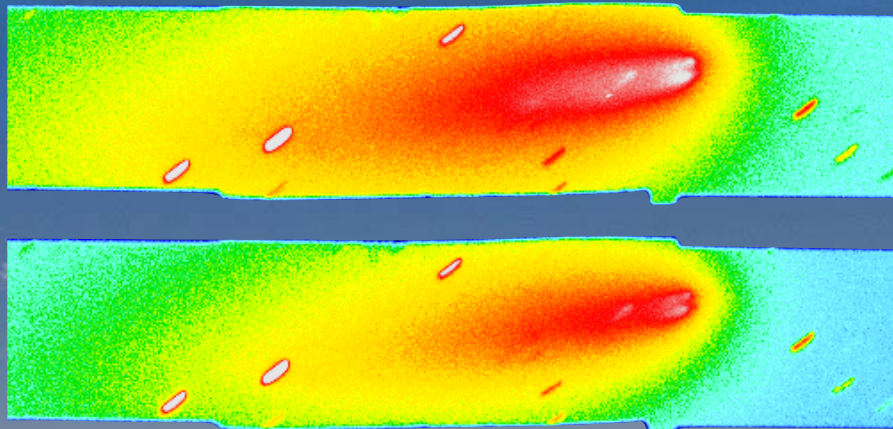
Polarimetry and spectropolarimetry of comet C/2013 R1 (LoveJoy)



Polarimetry and spectropolarimetry of comet C/2013 R1 (LoveJoy)



Thank you for your attention!



With better instrumentation
and
collaboration
to better science!